European Journal of Radiology 196 (2026) 112675

Contents lists available at ScienceDirect

European Journal of Radiology

journal homepage: www.elsevier.com/locate/ejrad

Research article

Ultrashort echo time MRI radiomics as a predictor of clinical outcomes in patellar tendinopathy: Insights from a large prospective clinical trial

Yijie Fang [a,b], Jie Deng [b,c], Stephan J. Breda [d], Robert-Jan de Vos [c], Edwin H.G. Oei [b], Jukka Hirvasniemi [b,e,*]

[a] Department of Radiology, The Fifth Affiliated Hospital of Sun Yat-sen University, Zhuhai, China
[b] Department of Radiology and Nuclear Medicine, Erasmus MC University Medical Center, Rotterdam, the Netherlands
[c] Department of Orthopedics and Sports Medicine, Erasmus MC University Medical Center, Rotterdam, the Netherlands
[d] Department of Radiology, AZ Turnhout, Belgium
[e] Department of Biomechanical Engineering, Delft University of Technology, Delft, the Netherlands

ARTICLE INFO

Keywords:
Jumper's knee
Ultrashort echo time
Radiomics
Machine learning
Predictive model
Deep learning segmentation

ABSTRACT

Purpose: To evaluate the predictive utility of radiomic features extracted from ultrashort echo time (UTE) MRI in comparison to conventional proton density (PD) sequences for short-term (24-week) and long-term (5-year) clinical outcomes in patients with patellar tendinopathy (PT) receiving exercise therapy.

Materials and methods: This prospective study of 76 PT patients undergoing 24-week exercise therapy underwent baseline 3D UTE and PD MRI at 3.0 T. The patellar tendon segmentation used nnU-Net, evaluated with Dice coefficient. Six predictive models consisting of clinical covariates and radiomic features from UTE and PD were developed using Elastic Net with 10-fold cross-validation. Model performance in predicting responsiveness of the patient-reported Victorian Institute of Sports Assessment (VISA-P) score was evaluated using the area under the receiver operating characteristic curve (ROC AUC) and the precision-recall curve (PR AUC), with 95% confidence intervals.

Results: The mean Dice similarity coefficient for the automatic segmentation of the patellar tendon from 3D-PD was 0.92 (SD: 0.02) and from 3D-UTE-Cones 0.89 (SD: 0.03). The UTE-based radiomics model demonstrated the highest predictive performance at 24 weeks (ROC AUC: 0.714 [95% CI: 0.701–0.727]; PR AUC: 0.848 [0.837–0.858]), while the PD-based model showed the lowest (ROC AUC: 0.569 [0.553–0.584]; PR AUC: 0.710 [0.692–0.727]). At the 5-year follow-up, UTE radiomics maintained robust performance (ROC AUC: 0.692 [0.677–0.706]; PR AUC: 0.822 [0.810–0.834]), whereas PD radiomics remained limited (ROC AUC: 0.578 [0.561–0.594]; PR AUC: 0.694 [0.676–0.713]).

Conclusions: Radiomics features extracted from UTE MRI demonstrate the highest predictive performance for clinical outcomes.

1. Introduction

Patellar tendinopathy (PT) is a common sports-related injury, with a reported prevalence of approximately 18% among athletes [1]. Clinically, PT is characterized by localized pain at the inferior pole of the patella, typically provoked by mechanical loading activities such as jumping, running, or squatting. The underlying pathology involves disorganization of the tendon tissue structure, including disrupted collagen alignment, increased ground substance, and neovascularization. This disease is often characterized by persistent symptoms and reduced function. According to a previous study of 77 athletes with patellar tendinopathy, 58% of the athletes had difficulties in physically demanding work [2]. Although exercise therapy is widely regarded as the first-line treatment, substantial variability in clinical

Abbreviations: PT, Patellar tendinopathy; ML, Machine learning; AI, artificial intelligence; UTE, ultrashort echo time; PTLE, the efficacy of progressive tendon-loading exercises; EET, eccentric exercise therapy; VISA-P, Victorian Institute of Sports Assessment–Patella; ROC, Receiver operating characteristic curves; PR, precision-recall curves; AUC, area under the curve.

* Corresponding author at: Department of Radiology & Nuclear Medicine, Erasmus MC University Medical Center, P.O. Box 2040, 3000 CA Rotterdam, the Netherlands.

E-mail address: j.hirvasniemi@erasmusmc.nl (J. Hirvasniemi).

https://doi.org/10.1016/j.ejrad.2026.112675
Received 24 September 2025; Received in revised form 10 December 2025; Accepted 13 January 2026
Available online 14 January 2026

outcomes has been observed. Several studies have indicated that treatment type, pain severity and location, patellar height, and imaging findings could be associated with clinical outcomes [3–8]. Developing a prognostic model is one strategy that might help clinicians predict who is at risk of poor prognosis and help guide individualized intervention strategies.

Machine learning (ML), a subset of artificial intelligence (AI), has shown considerable potential in tendon research, demonstrating efficacy in diagnosis, monitoring disease progression, and predicting prognosis by analyzing complex, multi-dimensional datasets [9–11]. Among the various input modalities used in ML models, imaging data have proven especially valuable. Tendons are tissues with short T2, with transverse relaxation times on the order of a few milliseconds or less [12]. This inherent physical property causes them to generate minimal signal and appear nearly "invisible" on conventional MRI sequences [13]. As a result, common sequences such as proton density (PD), and T2-weighted images are limited to visualizing gross late-stage abnormalities such as thickening or tears, rather than the early microstructural alterations crucial for timely diagnosis [5]. Consequently, most existing tendon-related ML studies utilize conventional MRI sequences, limiting their ability to capture early pathological changes and potentially reducing the model accuracy. In contrast, ultrashort echo time (UTE) MRI, with sub-millisecond echo times, enables improved visualization of short T2 tissues. Evidence that UTE-T2* correlates with symptomatic severity and treatment response in patellar tendinopathy [6,14] shows its potential to identify and objectively quantify the early collagen disorganization characteristic of tendinopathy. Radiomics enables the extraction of quantitative features from medical images that may not be visible to the human eye, transforming them into data that can be used to develop models for more accurate diagnosis, prognosis, and prediction [15]. Consequently, radiomic features extracted from UTE sequences may offer superior prognostic value compared to those obtained from conventional sequences. However, no prior studies have evaluated whether radiomic features extracted from UTE MRI outperform those from conventional PD sequences in predicting both short- and long-term clinical outcomes in patients with tendinopathy.

Therefore, the objective of this study was to evaluate the utility of MRI-based radiomic features in predicting both short-term (24-week) and long-term (5-year) clinical outcomes in patients with PT undergoing exercise therapy, by comparing the performance of predictive models built from radiomic features extracted from UTE MRI sequences against those extracted from conventional PD sequences and models based on clinical data.

2. Materials and methods

2.1. Datasets

This study utilized baseline data from 76 athletes (58 men; mean age 24 ± 4 years) enrolled between January 2017 and June 2019 in the JUMPER trial, a randomized controlled trial (ClinicalTrials.gov ID: NCT02938143) comparing the efficacy of progressive tendon-loading exercises (PTLE) and eccentric exercise therapy (EET) in patients with patellar tendinopathy [7]. Participants were aged 18–35 years with a history of patellar tendon pain related to sports activity and performed sports at least three times weekly prior to symptom onset. Inclusion required tenderness at the proximal patellar tendon and the validated and disease-specific patient-reported Victorian Institute of Sports Assessment–Patella (VISA-P; 0–100 points) score below 80 points [16]. Diagnosis of patellar tendinopathy (PT) was based on clinical evaluation and ultrasonographic (US) assessment. The diagnosis was established by an experienced sports physician. The clinical examination was considered positive if pain at the inferior patellar pole or patellar tendon was provoked by palpation or during a single-leg squat. The US examination was performed by a radiologist-in-training with 5 years of experience. The ultrasound examination was considered positive when one or more of the following findings were present: structural abnormalities, hypoechoic changes, tendon thickening (anterior–posterior diameter > 6 mm), or intratendinous power Doppler signal [7]. Key exclusion criteria included absence of simultaneous axial 3D-UTE and 3D-PD imaging, presence of other knee pathologies identified by ultrasound or MRI, and prior joint injection therapy (Fig. 1). Details of these exercise programs can be found in a prior publication [7]. Ethical approval was obtained by the review board of Erasmus MC University Medical Center (NL58512.078.016), and all participants provided written informed consent.

At the 24-week follow-up, 18 participants were lost, resulting in 58 athletes (76%) included in the interim analysis. At the 5-year follow-up, a total of 25 participants were lost, and 51 athletes (67%) remained for the final analysis (Fig. 1). Demographic characteristics of the study population are presented in Table 2.

2.2. Predicted outcome

Clinical outcomes were collected at baseline, 24 weeks, and 5 years. Pain-related disability was assessed using the VISA-P questionnaire [7]. A higher score represents a lower level of disability. The change in VISA-P score was further dichotomized into clinical responsiveness (≥14 points) and non-responsiveness (<14 points) with the threshold determined by the minimal clinically important difference [MCID] [17].

2.3. Clinical predictors

Several clinical predictors were collected at baseline as follows: 1) Visual Analogue Score (VAS) after single-leg decline squat (VAS-SLDS) on a 0–10 point scale; 2) VISA-P score; 3) sports activity level measured by the Cincinnati Sports Activity Scale (CSAS) as well as sex, age, body mass index (BMI) and symptom duration.

2.4. Image acquisition

MRI scanning was performed at baseline with a 3.0 T scanner (Discovery MR750, GE Healthcare, Waukesha, WI, USA) using a 16-channel flexible coil (NeoCoil, Pewaukee, WI, USA) and a fixation device. The knee was positioned at 30° flexion, using a cylindrical tube and foam padding [18]. The center-spot of the coil was aligned with the inferior patellar border. Acquisition was initiated with a sagittal 3D PD fast spin echo sequence of the knee, which was subsequently used to create precise localizer images to prescribe further acquisitions aligned with the direction of the collagen fibers of the patellar tendon. The patellar tendon was scanned in the axial plane using the 3D-UTE-Cones sequence, which is a gradient-echo-based acquisition using radial readout of the k-space. A total of 16 echoes were acquired in four separate multi-echo sequences containing four echoes in interleaved order. For each multi-echo acquisition, the same repetition time (TR) was used. The full protocol for sequence parameters in this study is listed in Table 1.

2.5. Automatic segmentation of patellar tendon

Two deep learning nnU-Net models (version 2) were trained to automatically segment patellar tendon from both 3D-PD and 3D-UTE-Cones (TE = 0.97) sequences separately [19]. The models were trained using 5-fold cross-validation, 3D configuration, and for 1000 epochs. The training data consisted of patellar tendons of 20 randomly selected participants. For model training, the patellar tendons were manually segmented on both sequences separately using ITK-SNAP software [20]. The volume of interest was confined to the volume between the inferior patellar pole and the tibial tuberosity (Fig. 2C&D).

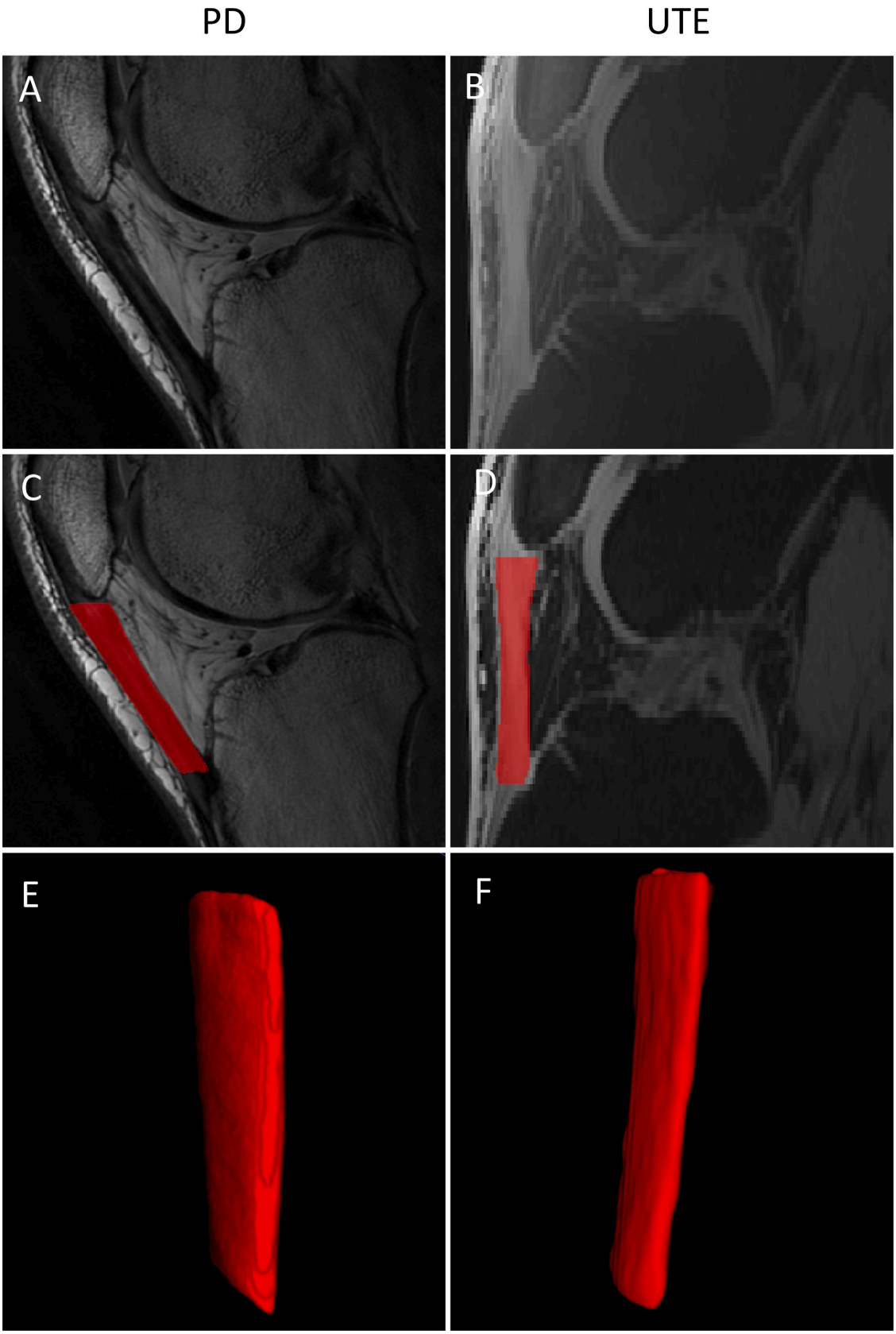

Fig. 1. The flow diagram. UTE = Ultrashort echo time.

Table 1
Parameters of the magnetic resonance imaging protocol.

Sequence	3D PD Cube	3D ME-UTE
Matrix	384 × 384	252 × 252
Scan plane	Sagittal	Axial oblique
FOV (cm)	15.0	15.0
Slice Thickness (mm)	1.0	1.5
Number of Slices	120	60
TE (ms)	30.0	0.032/4.87/12.67/20.47 0.49/6.82/14.62/22.42 0.97/8.77/16.57/24.37 2.92/10.72/18.52/26.32
TR (ms)	1200.0	83.4
Bandwidth (±kHz)	83.33	125
NEX	0.5	1.0
Flip Angle (°)	–	17
Fat saturation	No	Yes
Scan Time (mm: ss)	03:17	13:15

PD = Proton density, ME = multi-echo, UTE = ultra-short echo time, FOV = field-of-view, FS = fat saturation, TE = echo time, TR = repetition time, NEX = number of excitations.

2.6. Radiomics

Radiomic features of the segmented patellar tendon were calculated using the open-source Workflow for Optimal Radiomics Classification package (v. 3.6.2) in Python [21]. 13 histogram-based features and 376 texture features were extracted from 3D-PD and 3D-UTE-Cones (TE = 0.032) data separately (Supplementary Table 1). Texture features included local binary patterns, gray level co-occurrence matrix (GLCM), and GLCM multislice (GLCMMS), gray level run length matrix, gray level size zone matrix (GLSZM), neighborhood gray tone difference matrix, and Gabor features.

2.7. Statistical analyses

To assess the accuracy of the automatic segmentation, the Dice similarity coefficient was calculated in the validation set of each of the 5 nnU-Net training folds. The Dice coefficient quantifies the overlap between automatically and manually segmented patellar tendons. It ranges from 0 to 1, with higher value indicates better segmentation accuracy. Machine learning was used for dimensionality reduction and to evaluate the predictive utility of radiomic features from the patellar tendon in forecasting short- and long-term clinical outcomes in patients with patellar tendinopathy (PT) undergoing exercise therapy. Six different models were created: Model 1: 3D-UTE-Cones features model; Model 2: 3D-PD features model; Model 3: clinical covariate model that included CSAS, VAS, sex, age, BMI, duration of symptoms and different exercise treatment groups (PTLE and EET); Model 4: combined clinical covariate + 3D-UTE-Cones features model; Model 5: combined 3D-UTE-Cones + 3D-PD features model; Model 6: combined clinical covariate + 3D-UTE-Cones + 3D-PD features model. Dimensionality reduction and classification were performed using Elastic Net regression, a regularized logistic regression method that linearly combines the L1 and L2 penalties of Lasso and ridge regression. To optimize the ratio of the L1 and L2 penalties (α) and the strength of the penalty parameter (λ) of the Elastic Net, 10-fold cross-validation with a grid search and 100 repetitions was performed. In the grid, the values of α varied from 0.1 to 1 with an increment of 0.05 and λ from 0.001 to 0.15 with an increment of 0.009. When α is close to 0, the Elastic Net approaches ridge regression, while when α is 1, Lasso regression is performed. In cross-validation, the performance of the aforementioned six models to predict the VISA-P score was assessed using the area under the receiver operating characteristic (ROC AUC) and precision-recall curves (PR AUC) along with 95% confidence intervals (CI) [22]. As additional measures, sensitivity, specificity and Youden's cutoff were also calculated. The Elastic Net experiments were done using the R software (version 3.5.2) with Caret, PRROC, glmnet, and pROC packages [23].

3. Results

At 24 weeks follow-up, 39 out of 58 patients (67.2%) achieved a treatment response, while at the 5-year follow-up, 33 out of 51 patients (64.7%) maintained a successful outcome. The baseline characteristics of patients are presented in Table 2. There were no significant differences in the baseline characteristics between completers (n = 51) and

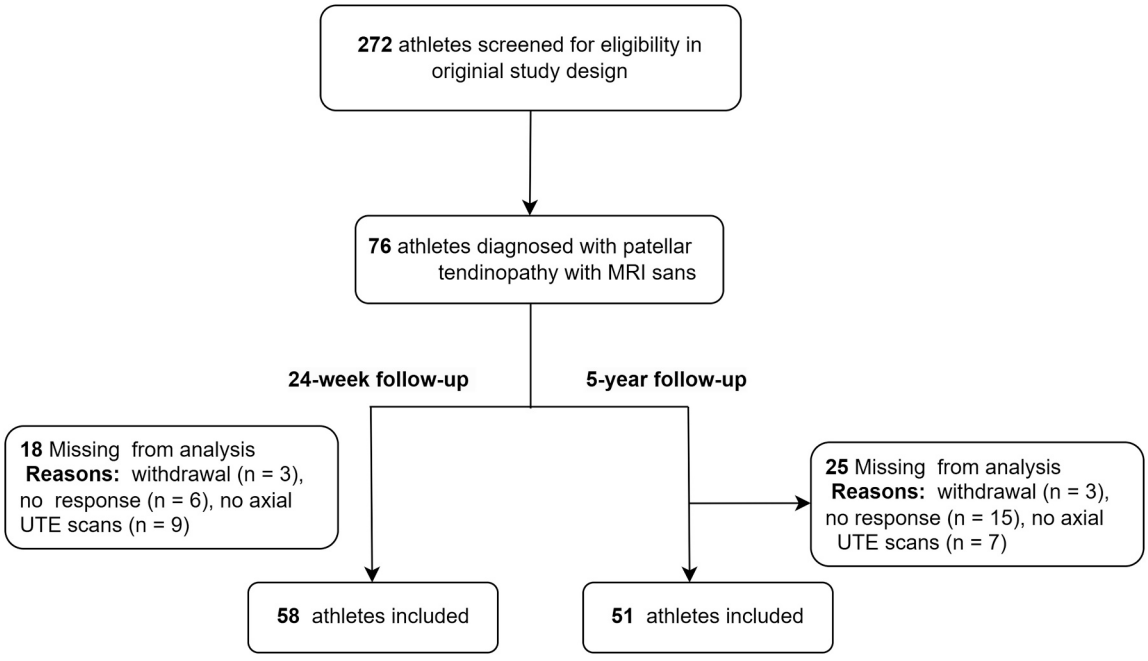

Fig. 2. Examples of automatic segmentation of the patellar tendon. (A) 3D proton density (PD) cube image and (B) 3D ultrashort echo time (UTE)-Cones image (TE = 0.032 ms) of the patellar tendon. (C) Segmentation of the patellar tendon from the 3D PD image and (D) from 3D UTE image. (E) 3D volumes of interest (VOIs) from the 3D PD scan and (F) from the 3D UTE scan.

dropouts (n = 25) (Supplementary Table 3).

The mean Dice similarity coefficient for the automatic segmentation of the patellar tendon from 3D-PD was 0.92 (SD: 0.02) and from 3D-UTE-Cones 0.89 (SD: 0.03) (Fig. 2).

With VISA-P score at 24 weeks as the outcome, the model utilizing radiomics features extracted from the 3D UTE MRI data achieved the highest predictive performance with ROC AUC of 0.714 (95% CI: 0.701–0.727) and a PR AUC of 0.848 (95% CI: 0.837–0.858). It outperformed 5 alternative models. Notably, the model based on 3D PD-derived radiomics showed the lowest performance with ROC AUC of 0.569 (95% CI: 0.553–0.584) and a PR AUC of 0.710 (95% CI: 0.692–0.727). Comparative results are detailed in Table 3, Supplementary Table 4, and Fig. 3. The optimized hyperparameters and the five variables with largest coefficients in the best performing Elastic Net models are shown in Supplementary Table 2.

A similar trend was observed when predicting VISA-P scores at the 5-year follow-up. The model based on radiomics features extracted from 3D UTE sequences achieved the highest performance, with an ROC AUC of 0.692 (95% CI: 0.677–0.706) and a PR AUC of 0.822 (95% CI: 0.810–0.834). The full integration model yielded a comparable ROC AUC of 0.692 (95% CI: 0.676–0.707), but with a slightly lower PR AUC of 0.788 (95% CI: 0.772–0.802). These models outperformed both the combined UTE/PD radiomics model and the UTE radiomics plus clinical data model. In contrast, the standalone clinical model (ROC AUC: 0.545, 95% CI: 0.536–0.570; PR AUC: 0.645, 95% CI: 0.625–0.663) and the 3D PD radiomics model (ROC AUC: 0.578, 95% CI: 0.561–0.594; PR AUC: 0.694, 95% CI: 0.676–0.713) showed substantially lower predictive performance. Detailed comparisons are presented in Table 3, Supplementary Table 4, and Fig. 4.

4. Discussion

Based on the largest available dataset derived from a randomized controlled trial of patients with PT treated with exercise therapy, our study demonstrates that models based on radiomics features extracted from UTE sequences provide the highest performance for predicting patient-reported outcomes at both short-term and long-term follow-up. In contrast, models constructed using features extracted from conventional PD sequences performed poorly. Furthermore, the inclusion of PD-extracted radiomic features in combination with other models reduced the predictive accuracy of most models to varying degrees.

The highest predictive performance of models based on UTE-extracted features can be attributed to the unique imaging characteristics of UTE sequences, particularly their sensitivity to short-T2 tissues such as cortical bone, tendons, ligaments, and menisci [12,18,24,25]. These tissues have extremely low mobile proton density (ρ_m) and very short T2 relaxation times, resulting in rapid signal decay after the excitation pulse and minimal or no signal contribution to K-space [12]. Consequently, these tissues often appear as signal-void regions in conventional long TEs sequences (such as fast spin-echo PD or T2 sequences), limiting the detection of early pathological changes. Although PD-weighted imaging is widely used in musculoskeletal diagnostics, it primarily identifies late-stage pathological features, such as collagen disruption, edema, and mucoid degeneration, by highlighting hyperintense signals against a low-signal background [5]. However, in PT and other overuse-related diseases, substantial alterations in the extracellular matrix (ECM), such as collagen remodeling, accumulation of glycosaminoglycans occur before these late-stage imaging features manifest [26,27]. These early changes are often undetectable by conventional PD imaging, leading to significant information loss. In contrast, UTE sequences enable “whole-organ” imaging of short-T2 tissues, capturing subtle and diffuse signal alterations throughout the tissue matrix [13]. This facilitates the extraction of comprehensive radiomics features reflecting early ECM changes, thereby offering significant advantages over features extracted from conventional PD sequences.

Among all models evaluated, PD-based radiomics features consistently exhibited the lowest predictive performance in predicting VISA-P outcomes at 24 weeks after initiation of exercise therapy, even resulting in worse performance than models based solely on clinical data. Although previous literature has confirmed that PD imaging is widely used and supports effective diagnostic modeling for tendon lesions [28,29], it primarily captures mid- to late-stage pathology, limiting its utility for prognostic modeling. Additionally, including PD-extracted features decreased the performance of other models. The reduction in performance is not because PD features carry no biological information, but rather because their weak predictive signal is overshadowed by noise. Furthermore, the PD features may have introduced detrimental multicollinearity with the more comprehensive UTE features, particularly within the constraints of our sample size, thereby diluting the contribution of UTE-based radiomics and some clinical features [30]. This highlights the need for caution when selecting input MRI sequences for AI predict modeling in musculoskeletal applications involving short-T2 tissues, as long-TE sequences such as PD may compromise model performance.

At the 5-year follow-up, models based on UTE sequences maintained the highest predictive efficacy, albeit with a slight performance reduction compared to the 24-week assessment. This difference could be partially attributable to the increasing influence of unmeasured clinical confounders over the long term, such as variations in rehabilitation adherence, training consistency, and mid-study treatment modifications, which are likely strong determinants of ultimate recovery [31]. However, beyond the accumulation of these factors, the performance difference may fundamentally reflect the distinct biological processes captured at each timepoint. The 24-week outcomes probably represent a composite of early inflammatory changes and the initial tissue response to exercise therapy. In contrast, the 5-year outcomes are more likely driven by long-term tendon remodeling, adaptation, and the cumulative effect of factors such as sustained loading and aging. The sustained predictive power of the UTE model at this stage implies that it captures enduring structural properties of the tendon. Our findings suggest that UTE radiomics features are sensitive to the pathophysiological state of the tendon. The higher performance at 24 weeks could indicate that these features are particularly adept at characterizing the early, more dynamic phase of treatment response. The sustained, albeit somewhat diminished, predictive power at 5 years implies that these features also capture enduring structural properties of the tendon that influence long-

Table 2
Comparison of baseline clinical characteristics between patients completing 24-week follow-up vs 5-year follow-up.

		24-w baseline data (n = 58)	5-y baseline data (n = 51)
Age (years)		24.0 (21.3–27.0)	24.0 (22.0–27.0)
Sex	Male	44 (75.9%)	38 (74.5%)
	Female	14 (24.1%)	13 (25.5%)
BMI		23.7 (22.1–25.4)	23.6 (22.1–25.1)
Treatment	PTLE	31 (53.4%)	27 (52.9.5%)
	EET	27 (46.5%)	24 (47.1%)
CSAS sports activity level	Level 1: 4–7 d/wk	14 (24.1%)	12 (23.5%)
	Level 2: 1–3 d/wk	44 (75.9%)	39 (76.5%)
VISA_P score		57.0 (46.3–65.0)	58.0 (46.5–66.0)
VAS score		5.0 (3.0–6.8)	5.0 (3.0–7.0)
Duration of symptoms(weeks)		104 (40.0–195.0)	104 (52.0–234.0)

Data are expressed as medians with interquartile range in parentheses, or number of patients with the percentage in parentheses. BMI = body mass index, calculated as weight in kilograms divided by height in meters squared, CSAS = Cincinnati Sports Activity Scale, VISA-P = Victorian Institute of Sports Assessment–Patella, PTLE = progressive tendon-loading exercises, EET = eccentric exercise therapy, VAS = visual analogue scale, 24-w = 24 weeks,5-y = 5 years.

Table 3
Area under the receiver operating characteristic curve (ROC AUC) and area under the precision-recall curve (PR AUC) values to predict the VISA-P of 24 weeks and 5 years with the models using only covariates, image features, and the combined covariates and image features model.

VISA-P	AUC	Model 1	Model 2	Model 3	Model 4	Model 5	Model 6
24 weeks	ROC(95%CI)	0.714 (0.701–0.727)	0.569 (0.553–0.584)	0.649 (0.633–0.664)	0.711 (0.697–0.725)	0.674 (0.659–0.689)	0.654 (0.638–0.669)
	PR(95%CI)	0.848 (0.837–0.858)	0.710 (0.692–0.727)	0.740 (0.723–0.756)	0.837 (0.825–0.848)	0.797 (0.783–0.812)	0.784 (0.770–0.800)
5 years	ROC(95%CI)	0.692 (0.677–0.706)	0.578 (0.561–0.594)	0.545 (0.536–0.570)	0.691 (0.677–0.706)	0.688 (0.672–0.704)	0.692 (0.676–0.707)
	PR(95%CI)	0.822 (0.810–0.834)	0.694 (0.676–0.713)	0.645 (0.625–0.663)	0.813 (0.800–0.825)	0.780 (0.763–0.794)	0.788 (0.772–0.802)

VISA-P: Victorian Institute of Sports Assessment–Patella.
Model 1: 3D-Ultrashort Echo Time (UTE) features model.
Model 2: 3D-Proton Density (PD) features model.
Model 3: Clinical covariate model.
Model 4: Combined clinical covariate + 3D-UTE-Cones features model.
Model 5: Combined 3D-UTE-Cones + 3D-PD features model.
Model 6: Combined clinical covariate + 3D-UTE-Cones + 3D-PD features model.

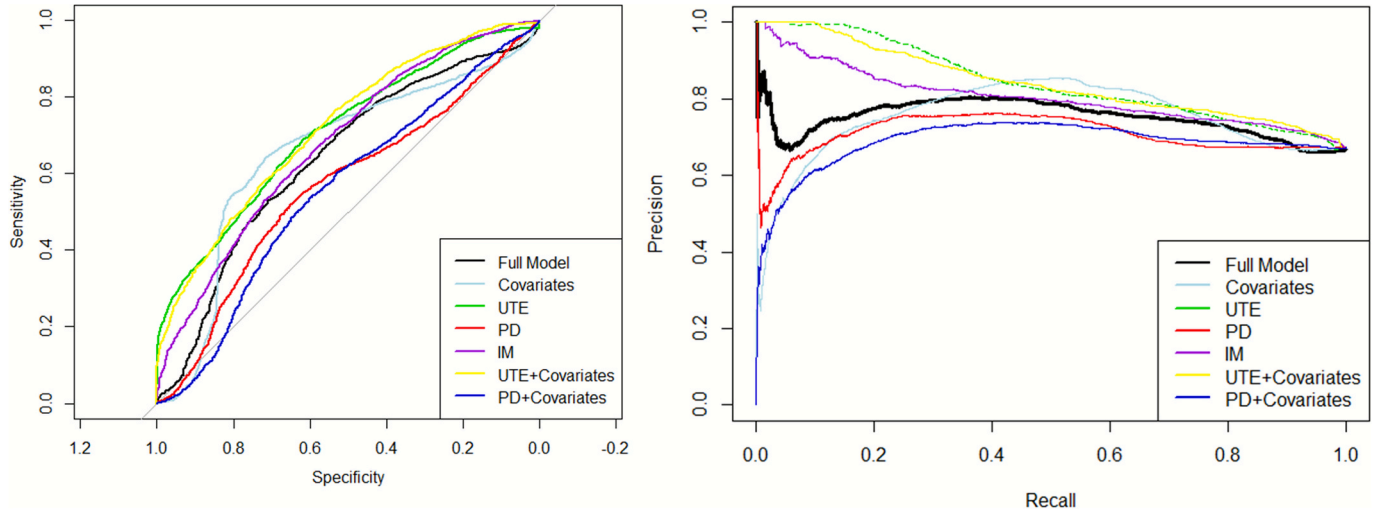

Fig. 3. Receiver operating characteristic (ROC) and precision-recall (PR) curves, along with corresponding area under the curve (AUC) values, were used to evaluate model performance in predicting 24-week VISA-P outcomes in PT patients. Models included covariates, PD, and UTE imaging radiomics features from volumes of interest, as well as combined models integrating both clinical covariates and imaging radiomics features.

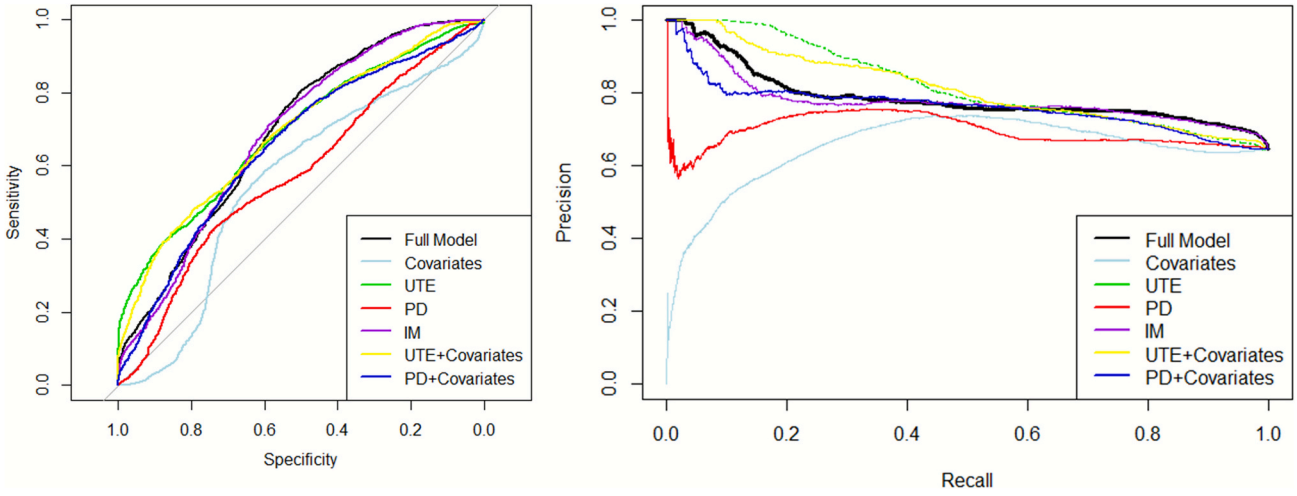

Fig. 4. Receiver operating characteristic (ROC) and precision-recall (PR) curves, along with corresponding area under the curve (AUC) values, were used to evaluate model performance in predicting 5-year VISA-P outcomes in PT patients. Models included covariates, PD and UTE imaging radiomics features from volumes of interest, as well as combined models integrating both clinical covariates and imaging radiomics features.

term clinical outcomes.

Gabor features and GLCM-based homogeneity index were present in the UTE models for both 24 weeks and 5 years. While linking the radiomic features to underlying pathophysiology is not straightforward, the Gabor features, which are sensitive to directional edges and repetitive patterns in image texture [32–34], likely capture the disorganization and loss of the parallel collagen fiber architecture that characterizes tendinopathy. A decrease in these directional patterns would be consistent with the pathological breakdown of collagen integrity. Conversely, the GLCM homogeneity index measures the uniformity of local intensity distributions [34]. The positive coefficient of this feature in our Elastic Net model indicates that a more homogeneous tendon texture on UTE-MRI is associated with clinical responsiveness. This can be interpreted as reflecting a more structurally intact and organized extracellular matrix, potentially indicative of less severe pathology with reduced areas of focal mucoid degeneration, neoangiogenesis, or fibrillar disruption. Thus, these features collectively suggest that individuals responsive to treatment have tendons that are microstructurally more organized and uniform.

This study has several limitations. The radiomic analysis was limited by the relatively limited sample size and the high dimensionality of the data, which may have increased the risk of overfitting. The absence of external validation and the single-center, single-scanner design further limit the generalizability of our findings. Additionally, while there were no significant differences in baseline characteristics between completers and dropouts, bias from loss to follow-up cannot be entirely ruled out. Nevertheless, it is important to note that this dataset represents the largest and longest follow-up cohort of its kind reported to date [31], providing a valuable foundational investigation. Given these limitations, future large-scale, multi-center, prospective studies are imperative to independently validate this model, assess its generalizability, and refine it before any clinical application can be considered. According to recent recommendation [35], for the limited sample size, we employed 10-fold cross-validation repeated 100 times, yielding stable and reliable results. These findings further validate the feasibility and robustness of predicting VISA-P scores using radiomics features extracted from UTE sequences. In this study, the region of interest was confined to the area between the inferior patellar pole and the tibial tuberosity, rather than the entire patellar tendon. Since our primary goal was to evaluate the utility of MRI sequences for machine learning prediction models targeting short T2 tissues, we took this more rigorous approach by minimizing potential cortical bone interference. This was essential because both cortical bone and short T2 tissues exhibit ultra-short T2 signals and cannot be reliably distinguished using conventional proton density (PD) or ultrashort echo time (UTE) MRI sequences. Consequently, as our UTE-MRI-based model is the first of its kind for this prognostic task, a direct comparison with existing models is not feasible. By contrast, this limitation underscores the innovative contribution of our work and points to the need for future multi-modal studies to validate and compare its clinical value.

5. Conclusion

Our findings suggest that radiomics features from UTE sequences contain more predictive information than the features from PD sequences. Our findings also indicate that features from conventional long-TE sequences (e.g., PD imaging) may adversely impact model performance. Our results suggest that UTE-based radiomic models may have the potential to identify patients likely to respond to physical therapy. If validated in future studies, this approach could inform more personalized clinical decision-making, potentially helping to optimize treatment pathways and avoid prolonged, ineffective interventions.

CRediT authorship contribution statement

Yijie Fang: Writing – original draft, Validation, Methodology, Investigation, Conceptualization. **Jie Deng:** Writing – review & editing, Software, Data curation. **Stephan J. Breda:** Visualization, Data curation. **Robert-Jan de Vos:** Writing – review & editing, Methodology, Data curation. **Edwin H.G. Oei:** Writing – review & editing, Supervision, Conceptualization. **Jukka Hirvasniemi:** Writing – review & editing, Supervision, Software, Investigation.

Declaration of competing interest

The authors declare that they have no known competing financial interests or personal relationships that could have appeared to influence the work reported in this paper.

Appendix A. Supplementary data

Supplementary data to this article can be found online at https://doi.org/10.1016/j.ejrad.2026.112675.

References

[1] S. Nutarelli, C.M.T. da Lodi, J.L. Cook, L. Deabate, G. Filardo, Epidemiology of patellar tendinopathy in athletes and the general population: a systematic review and meta-analysis, Orthop. J. Sports Med. 11 (6) (2023) 23259671231173659.
[2] A.J. De Vries, W. Koolhaas, J. Zwerver, et al., The impact of patellar tendinopathy on sports and work performance in active athletes, Res. Sports Med. 25 (3) (2017) 253–265.
[3] J.A. Kettunen, M. Kvist, E. Alanen, U.M. Kujala, Long-term prognosis for jumper's knee in male athletes. a prospective follow-up study, Am. J. Sports Med. 30 (5) (2002) 689–692.
[4] M. Gemignani, F. Busoni, M. Tonerini, M. Scaglione, The patellar tendinopathy in athletes: a sonographic grading correlated to prognosis and therapy, Emerg. Radiol. 15 (6) (2008) 399–404.
[5] M. Golman, M.L. Wright, T.T. Wong, et al., Rethinking patellar tendinopathy and partial patellar tendon tears: a novel classification system, Am. J. Sports Med. 48 (2) (2020) 359–369.
[6] S.J. Breda, R.J. de Vos, D.H.J. Poot, et al., Association between T(2)(*) Relaxation times derived from ultrashort echo time MRI and symptoms during exercise therapy for patellar tendinopathy: a large prospective study, J. Magn. Reson. Imaging 54 (5) (2021) 1596–1605.
[7] S.J. Breda, E.H.G. Oei, J. Zwerver, et al., Effectiveness of progressive tendon-loading exercise therapy in patients with patellar tendinopathy: a randomised clinical trial, Br. J. Sports Med. 55 (9) (2021) 501–509.
[8] H. Visnes, L.K. Bache-Mathiesen, T. Yamaguchi, et al., Long-term prognosis of patellar tendinopathy (Jumper's knee) in Young, Elite volleyball players: tendon changes 11 years after baseline, Am. J. Sports Med. 52 (13) (2024) 3314–3323.
[9] G. Droppelmann, C. Rodríguez, D. Smague, C. Jorquera, F. Feijoo, Deep learning models for tendinopathy detection: a systematic review and meta-analysis of diagnostic tests, EFORT Open Rev. 9 (10) (2024) 941–952.
[10] D. Muir, A. Elgebaly, W.J. Kim, et al., Predictive utility of the machine learning algorithms in predicting tendinopathy: a meta-analysis of diagnostic test studies, Eur. J. Orthop. Surg. Traumatol. 35 (1) (2025) 73.
[11] L. Thomas, J.H. Chung, S. Lu, A. Essilfie, Machine learning used to determine features of importance linked to overnight stay after patellar tendon repair, J. Orthop. 57 (2024) 55–59.
[12] M.D. Robson, P.D. Gatehouse, M. Bydder, G.M. Bydder, Magnetic resonance: an introduction to ultrashort TE (UTE) imaging, J. Comput. Assist. Tomogr. 27 (6) (2003) 825–846.
[13] J. Du, G.M. Bydder, Introduction to MRI of Short- and ultrashort-T2 tissues, in: J. Du, G.M. Bydder (Eds.), MRI of Short- and Ultrashort-T2 Tissues: Making the Invisible Visible, Springer International Publishing, Cham, 2023, pp. 3–10.
[14] A.S. Agergaard, R.B. Svensson, R. Hoeffner, et al., Mechanical properties and UTE-T2* in Patellar tendinopathy: the effect of load magnitude in exercise-based treatment, Scand. J. Med. Sci. Sports 31 (10) (2021) 1981–1990.
[15] R.J. Gillies, P.E. Kinahan, H. Hricak, Radiomics: images are more than pictures, They Are Data. Radiol. 278 (2) (2016) 563–577.
[16] J. Zwerver, T. Kramer, I. van den Akker-Scheek, Validity and reliability of the Dutch translation of the VISA-P questionnaire for patellar tendinopathy, BMC Musculoskelet. Disord. 10 (2009) 102.
[17] J. Deng, S.J. Breda, D. Eygendaal, E.H. Oei, R.J. de Vos, Association between physical tests and patients-reported outcomes in athletes performing exercise therapy for patellar tendinopathy: a secondary analysis of the JUMPER study, Am. J. Sports Med. 51 (13) (2023) 3523–3532.
[18] S.J. Breda, D.H.J. Poot, D. Papp, et al., Tissue-specific T(2) * biomarkers in patellar tendinopathy by subregional quantification using 3D ultrashort echo time MRI, J. Magn. Reson. Imaging 52 (2) (2020) 420–430.
[19] F. Isensee, P.F. Jaeger, S.A.A. Kohl, J. Petersen, K.H. Maier-Hein, nnU-net: a self-configuring method for deep learning-based biomedical image segmentation, Nat. Methods 18 (2) (2021) 203–211.

[20] P.A. Yushkevich, J. Piven, H.C. Hazlett, et al., User-guided 3D active contour segmentation of anatomical structures: significantly improved efficiency and reliability, Neuroimage 31 (3) (2006) 1116–1128.
[21] M.P.A. Starmans, S.R. van der Voort, T. Phil, et al, Reproducible radiomics through automated machine learning validated on twelve clinical applications, arXiv: 2108.08618 (2021). https://doi.org/10.48550/arXiv.2108.08618.
[22] C. Nadeau, Y. Bengio, Inference for the generalization error, Adv. Neural Inf. Process Syst. 12 (2000) 307–313.
[23] J. Hirvasniemi, S. Klein, S. Bierma-Zeinstra, et al., A machine learning approach to distinguish between knees without and with osteoarthritis using MRI-based radiomic features from tibial bone, Eur. Radiol. 31 (11) (2021) 8513–8521.
[24] D. Zhu, W. Wu, W. Yu, et al., Ultrashort echo time magnetization transfer imaging of knee cartilage and meniscus after long-distance running, Eur. Radiol. 33 (7) (2023) 4842–4854.
[25] Y. Fang, D. Zhu, W. Wu, et al., Assessment of achilles tendon changes after long-distance running using ultrashort echo time magnetization transfer MR imaging, J. Magn. Reson. Imaging 56 (3) (2022) 814–823.
[26] N.L. Millar, K.G. Silbernagel, K. Thorborg, et al., Tendinopathy, Nat. Rev. Dis. Primers 7 (1) (2021) 1.
[27] Y. Fang, D. Zhu, J. Wei, et al., Collagen denaturation in post-run Achilles tendons and Achilles tendinopathy: In vivo mechanophysiology and magnetic resonance imaging, Sci. Adv. 10 (40) (2024) eado2015.
[28] D.J. Lin, M. Schwier, B. Geiger, et al., Deep learning diagnosis and classification of rotator cuff tears on shoulder MRI, Invest. Radiol. 58 (6) (2023) 405–412.
[29] M. Ni, Y. Zhao, L. Zhang, et al., MRI-based automated multitask deep learning system to evaluate supraspinatus tendon injuries, Eur. Radiol. 34 (6) (2024) 3538–3551.
[30] I. Guyon, A. Elisseeff, An introduction to variable and feature selection, J. Mach. Learn. Res. 3 (2003) 1157–1182.
[31] A.S. Agergaard, R.B. Svensson, N.M. Malmgaard-Clausen, S.P. Magnusson, Clinical outcomes and tendon structure at 3- to 4-Year follow-up after exercise-based treatment of patellar tendinopathy: a prospective study, Orthop. J. Sports Med. 12 (10) (2024) 23259671241280192.
[32] S.E. Grigorescu, N. Petkov, P. Kruizinga, Comparison of texture features based on Gabor filters, IEEE Trans. Image Process. 11 (10) (2002) 1160–1167.
[33] R.S. Lu, E. Denison, H. Denison, C. Cooper, M. Taylor, M.J. Bottema, Texture analysis based on Gabor filters improves the estimate of bone fracture risk from DXA images, Comput. Methods Biomech. Biomed. Eng. Imaging Vis. 6 (2018) 453–464.
[34] M.P.A. Starmans, S.R. van der Voort, J.M.C. Tovar, J.F. Veenland, S. Klein, W. J. Niessen, Radiomics: data mining using quantitative medical image features, in: Handbook of Medical Image Computing and Computer Assisted Intervention., Elsevier, 2020, pp. 429–456.
[35] O. Efthimiou, M. Seo, K. Chalkou, et al., Developing clinical prediction models: a step-by-step guide, BMJ 386 (2024) e078276.